

Electrical and Optical Modulation of a PEDOT:PSS-Based Electrochemical Transistor for Multiple Neurotransmitter-Mediated Artificial Synapses

Giovanni Maria Matrone, Ugo Bruno, Csaba Forró, Claudia Lubrano, Stefano Cinti, Yoeri van de Burgt, and Francesca Santoro*

Neuromorphic systems that display synaptic conditioning based on biochemical signaling activity have recently been introduced in the form of artificial synapses that are model devices to develop tissue-interfaced platforms. In this regard, biohybrid synapses promise adaptive neuron-integrated functions. However, these systems suffer from both molecular cross-talk as biological neural circuits signal transmission typically involves more than one neuromodulator, and unstable electronics wirings as complex architectures are required to interface the tissues. Moreover, whilst novel spiking circuits can work as artificial neurons, they only recreate the biological electrical signaling pathway while electrochemical signal transduction is required for inter-neuron communication. As such, artificial chemically-mediated synapses are essential to perform memory/learning computing functions. Herein, an electrochemical neuromorphic organic device (ENODE) working as an artificial synapse that overcomes electrochemical and readout interferences while it emulates two neurotransmitters synaptic weight modulation and their recycling machinery at the synaptic cleft is shown. Neuronal short- and long-term plasticity are replicated by transducing two separate neurotransmitter-mediated chemical signals into reversible and nonreversible variations of PEDOT:PSS conductance. By exploiting the electrochromic properties of PEDOT:PSS, an alternative optical monitoring strategy is introduced which promises stable multidevice readout from complex bio-hybrid interfaces. The platform emulates high-order biological processes such as intrinsic forgetting, memory consolidation, and neurotransmitter co-modulation. These brain-inspired functionalities herald the development of tissue-integrated neuromorphic systems that combine spiking (electrical neurons) and nonspiking (electrochemical synapses) elements, thus envisioning prosthetic bridges for neural engineering and regenerative medicine.


1. Introduction

Artificial intelligence applications often require neural networks featuring highly demanding computational density and energy consumption.^[1,2] As a response to these technological challenges, neuromorphic computing aims to emulate the structure and functions of the brain, in order to outperform conventional von Neumann architectures. On this account, spiking neural networks (SNNs) introduce a spikes-based communication mechanism among artificial neurons.

However, efficient strategies to establish such biologically-inspired communication in SNNs is still lacking, drastically limiting the allowed computing functions.^[3]

Furthermore, learning/memory functions of the brain are based on the so-called synaptic plasticity, enabling neurons to change the weight of the synaptic connections depending on the received external stimuli through neurotransmitter modulation.^[4] This mechanism allows biological neural networks (BNNs) to perform multiple operations, such as learning and computation, in an energy-efficient way.^[5]

Similarly, by featuring brain-inspired plasticity behavior, artificial neuromorphic devices enable parallel computing algorithms with low energy consumption and high reliability.^[6,7]

 The ORCID identification number(s) for the author(s) of this article can be found under <https://doi.org/10.1002/admt.202201911>

© 2023 The Authors. Advanced Materials Technologies published by Wiley-VCH GmbH. This is an open access article under the terms of the Creative Commons Attribution-NonCommercial License, which permits use, distribution and reproduction in any medium, provided the original work is properly cited and is not used for commercial purposes.

DOI: 10.1002/admt.202201911

G. M. Matrone, U. Bruno, C. Forró, C. Lubrano, F. Santoro
Tissue Electronics
Istituto Italiano di Tecnologia
Naples 80125, Italy
E-mail: f.santoro@fz-juelich.de
G. M. Matrone, Y. van de Burgt
Microsystems
Institute for Complex Molecular Systems
Eindhoven University of Technology
Eindhoven 5612AJ, The Netherlands

Indeed, over the last decade, artificial neuromorphic systems have been designed by exploiting memristive devices whose conductance can be modulated to emulate the signal transmission of a biological synapse.^[8,9] In this scenario, organic neuromorphic devices based on conductive polymers (CPs) have emerged in bio-integrated applications because of their biocompatibility and mixed conduction (electronic and ionic) suitable for physiological processes, biomolecules-mediated operation and integration with cells and tissue.^[10,11] Due to their peculiar doping/de-doping processes, organic mixed ionic-electronic semiconductors feature a large dynamic range, i.e., they allow conductance modulations in a window (between their highest and lowest states) that is larger than 2x their initial conductance value.^[12] They enable analog tuning which is ideal for parallel computing applications.^[13] One class of organic neuromorphic devices are based on organic electrochemical transistors (OECTs), which have lately shown the ability to modify their conductive state upon an external stimulation (i.e., electrical pulses at the gate electrode) and to retain this altered conditioning over time, resembling synaptic plasticity.^[7] In particular, when the active material is poly(3,4-ethylene-dioxythiophene):polystyrene sulfonate (PEDOT:PSS), the device operates in depletion mode and the application of a voltage bias at the gate electrode causes a de-doping of the film due to cations penetrating its bulk.^[14] This mechanism is reversed upon removal of the voltage bias. Employing high-frequency voltage pulses as inputs, the reversibility of the process is hindered so that cations accumulate inside the PEDOT channel causing a cumulative de-doping which emulates short-term depressive behavior (STD).^[15]

The evolution of such systems towards bio-integrated and synaptic biomimicking applications has led to the development of neurotransmitter-mediated artificial synapses, i.e., devices working with species that participate in the biological signaling mechanisms such as dopamine (DA).^[16] From these concepts, biohybrid synapses has been developed establishing a long-term plasticity relationship between the oxidation of dopamine (released by cells directly coupled with the active material) and

the memory state (conductance) of the organic neuromorphic device.^[17]

However, in a biological synapse multiple neurotransmitters participate to the signaling mechanisms.^[18,19] For instance, DA and serotonin (5-HT) are important neuromodulators contributing to the regulation of synaptic plasticity such as long-term potentiation (LTP) and depression (LTD).^[20–22] Thus, sophisticated and adaptable bio-hybrid interfaces actively interacting with neurons must be able to correctly identify interrelated biological cues such as the concentration and distribution of these neurotransmitters. As such, the first step towards these next-generation bio-hybrid systems is the design of artificial synapses mediated by multiple neurotransmitters which could be further integrated into SNNs. In this context, organic artificial synapses may serve to both enhance the inference and training of spiking networks and emulate specific synaptic functions.^[3]

Here, we engineer an artificial synapse by integrating a fluid chamber for the control of neurotransmitter solutions flow in an ENODE design. This platform is able to display short and long-term conditioning mediated by two neurotransmitters by exploiting their selective oxidation: a key biological computational primitive. We show that this weight modulation is reversible, and essential for implementation in artificial neural networks. We simultaneously monitor the conditioning electrically and optically, and demonstrate the coexpression of multiple neurotransmitters to emulate neuronal learning and forgetting patterns. Indeed, optical detection approaches have emerged in the last years due to their unprecedented flexibility for choosing regions of interest.^[23,24]

This work paves the way for sophisticated bio-hybrid neuromorphic interfaces, comprising array of mutually dependent devices that are controlled by multiple neurotransmitters resulting from a variety of physiological cues that can be closely monitored using noninvasive optical readouts.

2. Results and Discussion

2.1. Device Design and Opto-Electronic Characterization

An ENODE (Figure 1 and Figure S1, S2, Supporting Information) was fabricated as described in **Methods**. Here, the gate terminal represents the presynaptic end of the artificial synapse while the transistor channel acts as the post-synaptic terminal.^[17] The gate electrode has been exposed to two different neurotransmitters (DA and 5-HT) which can be oxidized upon the application of a gate bias (oxidation potential).^[17] This potential has been determined for each neurotransmitter through cyclic voltammetry (CV) (Methods and Figure S3, Supporting Information) as 0.3 V, 0.4 V (vs. Ag/AgCl), for DA and 5-HT, respectively which is also in agreement with previous results.^[25,26]

Additionally, chronoamperometry measurements (Figure S4, Supporting Information) were performed to determine the neurotransmitters' diffusion coefficients resulting as $2.4 \times 10^{-6} \text{ cm}^2 \text{ s}^{-1}$ and $1.9 \times 10^{-5} \text{ cm}^2 \text{ s}^{-1}$ for DA and 5-HT, respectively. Here, although DA and 5-HT have different diffusion coefficients, due to the neurotransmitters specific interaction at the surface of the PEDOT:PSS electrode, they both display a diffusion-controlled oxidation mechanism (Figure S4 and S5, Supporting Information).^[27]

U. Bruno
Dipartimento di Chimica
Materiali e Produzione Industriale
Università di Napoli Federico II
Piazzale Vincenzo Tecchio, 80, Napoli, NA 80125, Italy

C. Forró
Department of Chemistry
Stanford University
290 Jane Stanford Way, Chem-H/Neuroscience S285, Stanford, CA 94305, United States

C. Lubrano, F. Santoro
Faculty of Electrical Engineering and IT
RWTH Aachen
52074 Aachen, Germany

C. Lubrano, F. Santoro
Institute for Biological Information Processing-Bioelectronics
Forschungszentrum Juelich
52428 Aachen, Germany

S. Cinti
University of Napoli Federico II
Department of Pharmacy
School of Medicine and Surgery
Via D. Montesano 49, Napoli 80131, Italy

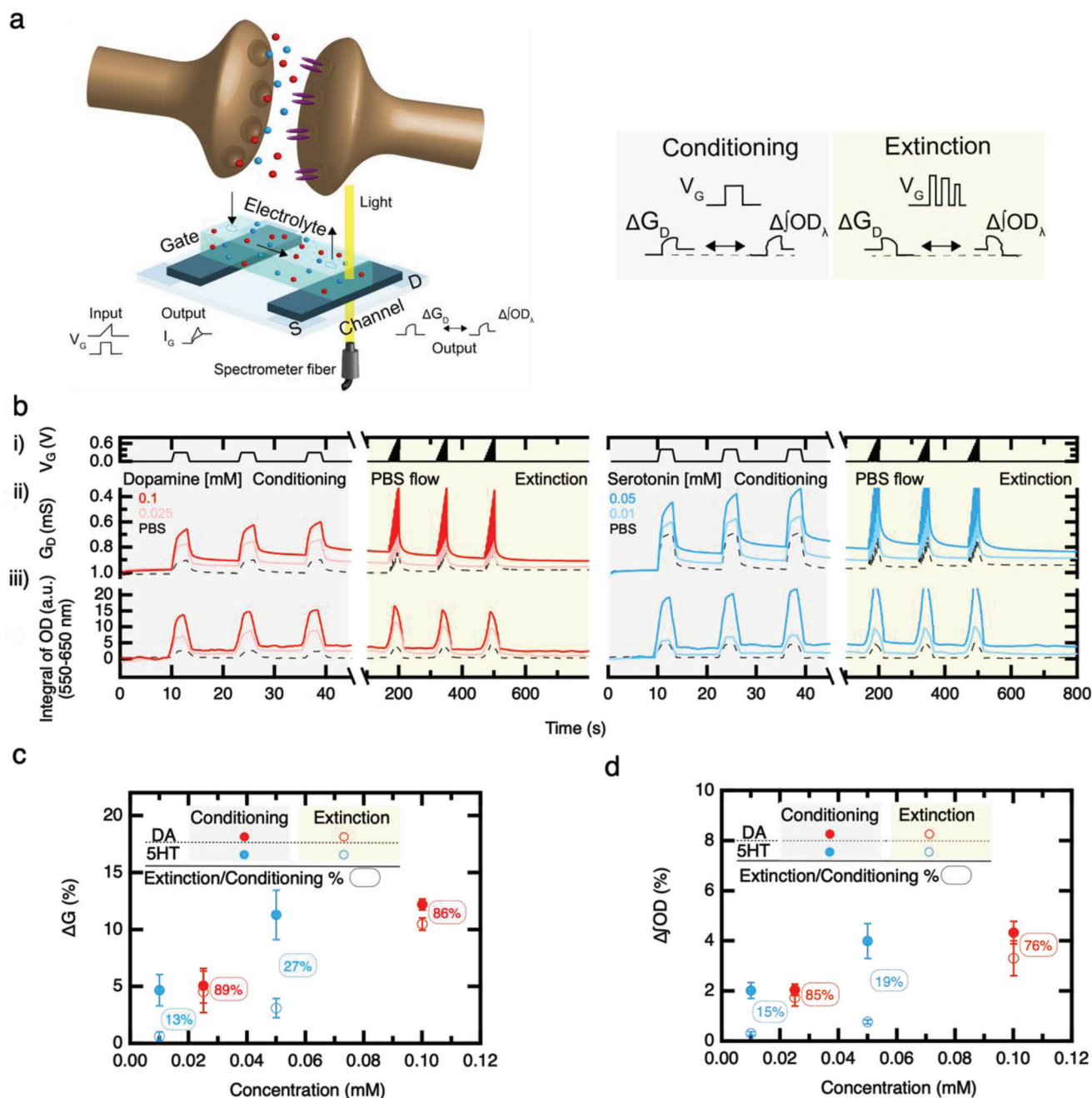


Figure 1. The artificial synapse: presynaptic and post-synaptic functions. a) Schematic illustrating the ENODE's gate electrode and the combination of the fluidic module and the channel terminal corresponding to the presynaptic and post-synaptic terminal of a biological synapse, respectively. b) Channel conductance modulation G_D (ii) and integral optical density changes $\int OD$ (iii) upon gate periodic voltage pulses (i) (three square pulses with 3s duration and 10s delay) that trigger the neurotransmitters oxidation (static PBS-neurotransmitter solution in the fluidic module), DA (left, red) and 5-HT (right, blue), followed by a baseline recovery input comprising three train of pulses (0.1 to 0.8 Vg, ΔV_G 0.1V, V_D -0.1 V) under PBS flow (1 mL min⁻¹). c) ΔG_D (%) (left) and d) $\Delta \int OD$ (%) (right) for both conditioning and extinction processes for the different concentrations of neurotransmitters. The % of the extinction/recovery ratios (hereafter named % of recovery, in rectangles) have been obtained from the ratio-to-percentage of extinction/conditioning values (ΔG_D % and $\Delta \int OD$ %). The initial conductance/integral of optical density baseline is partially recovered showing that the modulation triggered by DA is semi-reversible (>80% recovery) while 5-HT leads to more permanent modulations (<27% recovery).

Then, the long-term memory of the artificial synapse mediated by the individual neurotransmitters (Figure 1a) was characterized through the application of periodic voltage pulses (presynaptic signals at the gate electrode consisting of three-square pulses with 3 s duration and 10 s delay between pulses), whose amplitudes correspond to the previously determined neurotransmitter's oxidation potential (Figure 1b and Figure S3, Supporting Information).

The ENODE works as a depletion mode OECT: when a positive gate bias is applied cations from the electrolyte are injected into the channel terminal and compensate the anions on PSS[−] chains decreasing the number of holes and so the drain current (PEDOT:PSS de-doping).^[14] This leads to a reversible conductance modulation in case no neurotransmitters are present in the electrolyte solution (Figure 1bii, black dotted traces).

Here, in presence of a neurotransmitter, the PEDOT:PSS channel conductance decreases in a nonreversible way due to the de-doping process (Figure 1bii, red and blue solid traces).^[17] This mechanism is strongly influenced by protons and electrons produced during the oxidation reaction thus depending on the type of neurotransmitter and its concentration in the solution as previously shown.^[17]

In parallel, in situ time-resolved UV-vis measurements allow for monitoring the kinetics of penetrating ions in the polymer film^[28]: in the optical density (OD) spectrum, a new absorption peak at ≈ 650 nm is detected whose amplitude is increased by the de-doping process (Figure S6, Supporting Information). Optical readouts methods for PEDOT:PSS have been previously proposed,^[29] though here both electronical and optical measurements are simultaneously collected not only for material characterization but precisely for neuromorphic applications. The integral of optical density in the region 550–650 nm ($\int OD$) and its time-dependence have been extracted (Figures S6 and S7, Supporting Information) and compared to the channel conductance variations (Figures S8, S9, S10 and Table S1, Supporting Information), establishing a readouts correspondence: the same presynaptic signal elicits comparable variations of optical density and conductance (Figure 1biii) with respect to their relative baseline values, i.e., the readout values before the modulation (Figures S8, S10 and Tables S1, S2, Supporting Information).

Thus, both channel conductance and integral of optical density variations represent the modulation of the artificial synapse weight and as such correspond to the “memory of the device”: the neurotransmitters electrochemical signal is converted and stored through an opto-electronically readable and stable mechanism (ΔG_D , $\Delta \int OD$).

Interestingly, synapses operating with DA and 5-HT display specific modulations of ΔG_D and $\Delta \int OD$ (evaluated in percentages) so that the synapse conditioning is correlated to the specific neurotransmitter that has been employed as oxidizing species (Figures S8 and Table S1, Supporting Information) due to the distinct number of electrons and cations produced (Figure 1biii). This conditioning is also permanently retained due to the electrons produced and donated to the channel polymer, while simultaneously inducing the penetration of cations from the electrolyte to keep charge neutrality (Figure S8 and S9, Supporting Information).^[17,26] In terms of percentages of modulation, for the lowest concentration of DA and 5-HT (0.025 mM and 0.01 mM, respectively) the ratio between the electronic and optical mod-

ulations values is ≈ 2.3 – 2.5 (Table S1, Supporting Information), while for the higher concentrations (0.1 mM and 0.05 mM, respectively) the same ratio moves to 2.8.

Inspired by the mechanism of BNNs working to minimize their occupied storage by memory erasure and control processes,^[30,31] the intrinsic properties of PEDOT:PSS are here explored to reverse the de-doping process and possibly ‘erase’ a previously established conductance or optical density level (synaptic extinction following synaptic conditioning).

Here, the de-doping mechanism of the PEDOT:PSS channel can be reversed exploiting the un-binding of H⁺ from the PSS[−] domains (the mechanisms of doping/de-doping are explained in Figures S8 and S9, Supporting Information).^[32] To achieve this, in presence of electrolyte only, periodic voltage pulses have been applied with increasing amplitude (8 pulses of 3 s, delay 0 s, from 0.1 to 0.8 V, voltage step of 0.1 V) such that the penetrated cations can return to the electrolyte (extinction), restoring the initial conductance level of the transistor channel (Figure 1biii-iii).

Based on this, we observed that in the case of DA for both the examined concentrations (0.025 mM and 0.05 mM) the G_D and $\int OD$ modulations (5.07 and 12.21% of G_D and 2.04 and 4.33% of $\int OD$, respectively) increase with the neurotransmitter concentration in the conditioning phase. These modulation values have been extracted from the traces presented in Figure 1 (Figure S8 Supporting Information contains a detailed description of this analysis). The optical and electronical modulations can be partially reversed through the periodic gate pulses under PBS flow (extinction phase) achieving a recovery of the initial G_D and $\int OD > 75\%$ (Figure 1c,d, extinction/conditioning %). The percentages of the extinction/recovery ratios (hereafter named % of recovery) have been obtained from the ratio-to-percentage of extinction/conditioning values (Table S1, Supporting Information). In the case of DA, due to the efficient extinction mechanism (high values of % of recovery), the effects of a double cycle of conditioning/extinction phases have been investigated (Figure S11, Supporting Information). The artificial synapse, employing the lowest concentration of DA (0.025 mM), can allow repetitive cycles of learning/forgetting (Figure S16, Supporting Information).

5-HT solutions (0.01 mM and 0.05 mM, Figure 1b blue traces), after conditioning, lead to comparable values of G_D and $\int OD$ modulations (4.68 and 11.30% of G_D and 2.02 and 4.0% of $\int OD$, respectively) but induced a limited recovery of the conductance and integral of optical density (comprised in the window 10%–30%, Table S1, Supporting Information), suggesting a permanent long-term synaptic modulation.

In the case of 5-HT higher anodic current are recorded with a stronger de-doping of the polymer channel compared to the other neurotransmitter (Figures S3, S4, S5, Supporting Information). However, the % of recovery values extracted from the simultaneous opto-electronical monitoring almost coincide. Considering for example the DA 0.025 mM solution, the percentage of recovery values from the electronical and optical readout are 90% and 85%, respectively. Increasing the concentration of the neurotransmitters, only minor differences are encountered: these can be ascribed to the different rates at which the two species cause a fouling of the electrode in the static case. Whilst the two readout methods produce modulations values of different units which cannot be directly compared, the respective recovery percentages are close to being equal thus proving the intimate correspon-

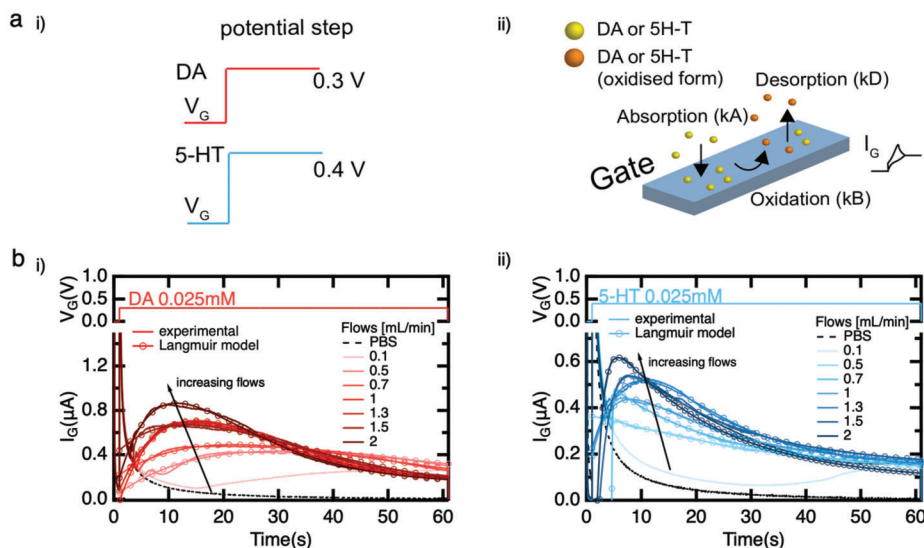


Figure 2. a) Schematics illustrating the amperometry experiments of panels b): i) a potential step matching the neurotransmitters oxidation potential is applied to the ENODE gate electrode. ii) The neurotransmitters molecules interact with the gate electrode through the mechanisms of absorption, oxidation, and desorption while the I_g current is monitored over time. b) I_g curves offers an insight into the diffusion of neurotransmitters towards the gate electrode in the fluidic channel depending on their initial concentration, DA (red) and 5-HT (blue). I_g traces are also fitted (circles) applying a Langmuir model that considers the neurotransmitters k_A (absorption), k_D (desorption), and k_B (oxidation) at the gate.

dence of the two monitoring approaches that are here confirmed to probe the same phenomena (PEDOT:PSS de-doping/doping, Figure S10, and Table S2, Supporting Information).

2.2. Dynamic Characterization of Neurotransmitter-Electrode Interaction

To achieve a fine control on the plasticity (conductance modulation) of the post-synaptic terminal, the fluid chamber integrated (Figure S1, Supporting Information) with the organic neuromorphic device was exploited to dynamically adjust the neurotransmitters' solution concentration over time. Here, the combined effect of the neurotransmitter diffusion and flow rate were investigated by monitoring the current at the gate electrode I_g while applying a constant gate bias that triggers the oxidation process (Figure 2ai,ii). A Langmuir model has been proposed in order to elucidate the artificial synapse's response (Figure S12, Supporting Information).^[33] The experimental I_g curves are replicated by this model's function (dotted circle in Figure 2bi,ii), highlighting that high flow regimes increase the number of species available for the oxidation while also preventing the gate electrode fouling caused by the reaction by-products, resulting in higher, sharper and faster occurring I_g peaks.

As such, in static and low flow-rate conditions (0 and 0.5 mL min⁻¹ flow, respectively) the neurotransmitters' oxidation is dominated by mass transport towards the electrode which leads to low values of I_g . On the other hand, the increase of the electrolyte flow causes the rise of the I_g maximum value due to a constant refresh of species available for the oxidation at the gate electrode.^[34]

However, high flow regimes (1.5 and 2 mL min⁻¹ for DA and 5-HT, respectively) affect the interaction of the neurotransmitters with the gate electrode, hindering the oxidation process (Figure 2bi-ii and Figure S10, Supporting Information).

In light of this, the neurotransmitters in solution induce a flow regimes-dependent modulation of the channel conductance and integral of optical density as reported in Figure 3bi,ii (for the complete statistics see also Figure S13 and Table S4, Supporting Information). Here, by applying the same periodic voltage pulses of the conditioning experiment (Figure 1bi), we determined the different neurotransmitters flow ranges that induce the maximum ΔG_D and $\Delta \int OD$ as 1 and 1.5 mL min⁻¹ for DA and 5-HT, respectively (Figure 3bi,ii and Table S4, Supporting Information).

Hence, the ΔG_D and $\Delta \int OD$ modulations flow regimes dependency can be exploited as a strategy to replicate DA and 5-HT molecules binding to post-synaptic receptors in the synaptic potentiated (large modulation) and depressed states (low modulation). Also, the devices proved to be stable for up to two weeks since their fabrication (Figure S13, Supporting Information).

2.3. Mimicking Biological Neurotransmitter Corelease Using the Artificial Synapse

Most neurons in the brain release more than one chemical working as a neuromodulator, each conveying a principal message, so the neural signaling mechanism is often regulated by the complex orchestration of multiple neurotransmitters.^[19] Here, the simultaneous presence of multiple neurotransmitters and their concurrent oxidation at the gate electrode is exploited to ultimately modulate the channel conductance (Figure 4a).

First, binary neurotransmitters solutions have been characterized through CV, transconductance, and differential pulsed voltammetry (DPV) measurements to evaluate possible interfering phenomena in their oxidation potentials previously evaluated individually (Figure S3,S14, S15,S16, Supporting Information).

Figure S15 (Supporting Information) shows the transconductance, CV and DPV traces that refers to binary solutions contain-

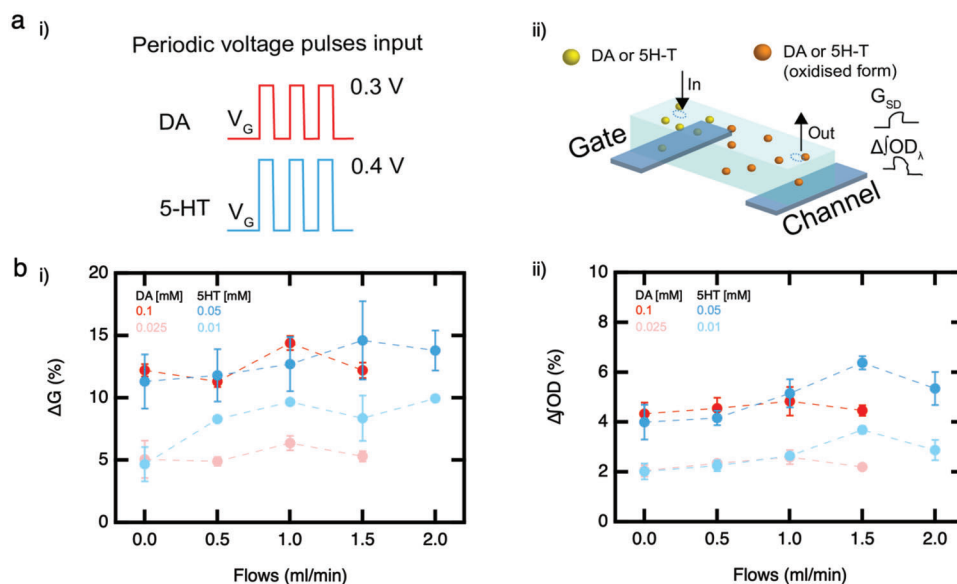


Figure 3. a) Schematics illustrating the periodic voltage pulses experiment of panels b: i) a periodic voltage pulses input (three square pulses with 3 s duration and 10 s of delay) matching the neurotransmitters oxidation potential is applied to the ENODE gate electrode, ii) The neurotransmitters enters the fluidic chamber (In) at a fixed flow rate, are oxidized at the gate electrode and exit the chamber (Out), while ΔG_D and ΔfOD are monitored. b) ΔG_D % (i) and ΔfOD % (ii), upon the periodic voltage pulses input, recorded from solutions containing different concentrations of DA (pulse amplitude 0.3 V) and 5-HT (pulse amplitude 0.4 V) at different flow rates (from 0, 0.5, 1, 1.5, 2 mL min⁻¹).

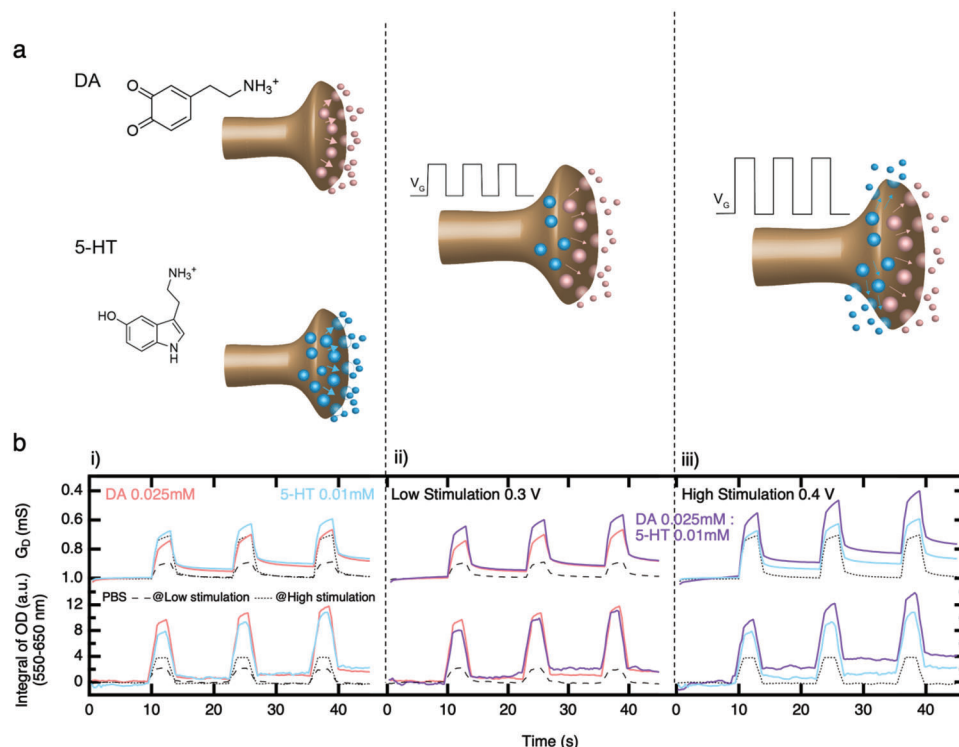


Figure 4. Neurotransmitter co-modulation. a) The schematic illustrates the release of neurotransmitters in case of single and double-neurotransmitters neurons, showing a coexpression process for high-stimulation presynaptic stimuli. b) i) The artificial synapse G_D and fOD modulations in case of DA (pink) and 5-HT (blue) at their respective oxidation potential, emulating a single neurotransmitters neuron. Black dotted curves represent the null G_D and fOD modulations in case of PBS-only solutions at low and high stimulation presynaptic stimuli, here used as reference. ii,) A double neurotransmitters neuron expressing the couple DA:5-HT 0.025:0.01mM under low stimulation, i.e. pulsing the gate at the DA oxidation potential (0.3 V). iii) The same neuron under high stimulation, pulsing the gate at the 5-HT oxidation potential (0.4 V).

ing DA:5HT (at different concentrations) in which two distinct peaks appear at 0.3 V and 0.4 V corresponding to the oxidation of DA and 5-HT, respectively, as previously reported.^[25]

The artificial synapse allows to tune its output response (to a fixed electrical input) through modulations (ΔG and $\Delta \int OD$) that can be controlled via chemical (type of neurotransmitters) and fluidodynamic means. Indeed, these are two methods to finely control the synaptic modulation and enable a wide range of different conditioning which allows this platform to reduce the gap with the programming capability of a biological synapse.

In this context, the artificial synapse's output depends on the amplitude of the voltage pulses used as input and serves to emulate the biological cotransmission mechanisms, as the neurotransmitters examined here are oxidizing at specific gate potentials.^[18,35]

Figure 4bi,ii,iii show the modulation of the ENODE in presence of diverse neurotransmitters binary solutions at the flow rate of 1 mL min⁻¹.

In case of DA:5-HT (0.025mM:0.01mM) mixture (Figure 4bii), the application of a low presynaptic stimulation corresponding to DA oxidation potential (0.3 V), results in electrical and optical modulations of the artificial synapse (6.21% of G_D and 2.7% of $\int OD$) comparable to the ones obtained for the solution with DA only (6.37% of G_D and 2.6% of $\int OD$) (Figure 4bi). By contrast, the application of a larger-synaptic input (Figure 4biii), corresponding to the 5-HT anodic potential (0.4 V), triggers the simultaneous oxidation of DA and 5-HT and results in large output modulations (10% of G_D and 4.7% of $\int OD$). These values are slightly lower than the arithmetic sum of the modulations obtained by the individual neurotransmitter's solution (DA+5-HT 15% of G_D and 5.2% of $\int OD$, Figure S13 and Table S4, Supporting Information), possibly due to minor interferences phenomena arising when the two species diffuse simultaneously towards the electrode interface where they compete for oxidation.^[27,36] Nevertheless, the selectivity of the oxidation mechanisms enables a voltage amplitude-dependent synaptic modulation that allows to prove the efficiency of the biological emulation process.

3. Conclusion

In this work, we presented an artificial synaptic platform based on a ENODE architecture with two neurotransmitters-mediated plasticity. We have proved that the synaptic weight modulation of this neuromorphic platform is reversible, and it depends not only on the concentration of neurotransmitters but also on the type of released neurotransmitters, allowing to emulate neuronal learning and forgetting patterns, and to replicate these biorelevant molecules binding to specific post-synaptic receptors varying in size, number, and distribution.

Crucially, the proposed approach that exploits the optical spectrum variations of PEDOT:PSS to evaluate the synaptic conditioning, paves the way to the use of spectroscopic techniques in engineering neuromorphic circuits such as SNNs.

A noninvasive optical array facilitates the bio-hybrid coupling with tissues while the correspondence between electronic (channel conductance, G_D) and optical (channel absorbance spectrum, specifically the integral of optical density, $\int OD$) modulation may be employed as a further strategy to control the SNNs

inter-neuronal communication enabling feedback regulated and memory/learning functions.

The neurotransmitter-specific synaptic plasticity combined with the reversibility of the process is able to transduce synaptic signals allowing it to pass from in vitro cultures comprising models of neuronal cells (PC-12 cells which express mainly DA) to cell cultures expressing multiple neurotransmitters.

Ultimately, SNNs comprising artificial neurons and artificial synapses are envisioned where the synaptic weight of each spiking element interconnection is selectively programmable, and the associated information may be intentionally stored.

Such spiking networks may include cascading neural pathways that perform sensory coding and signal propagation with a local modulation of neurons spiking activity. Hence, the optoelectronic readout with the reversible programming capabilities opens to previously unexplored learning/forgetting paradigms. These surpass in computing performance the conventional parallel programming standards by exploiting a bio-inspired signal processing which is i) neurotransmitter-selective, ii) combines multiple inputs and iii) dynamically adapts to the neuronal biological scenarios.

4. Experimental Section

ENODE Fabrication: The ENODE devices were fabricated on glass-ITO patterned substrates purchased from Xin Yan Technology Ltd. The size of the glass square substrates is 25 mm with patterned squares of ITO (20 ohm sq⁻¹) of 10 mm covering each corner. Substrates were cleaned through sonication in IPA (Sigma-Aldrich, USA) for 20 min. Employing Kapton tape and using a PMMA master mask, 2 stripes connecting opposed ITO squares (with fixed width 3 mm and length 20 mm) were traced for the deposition of the polymer mixture. PEDOT:PSS (Hereaus, Clevios PH 1000) aqueous solution was prepared by adding 6 vol.% ethylene glycol (Sigma-Aldrich, USA) to increase the PEDOT:PSS conductivity, 0.1 vol.% dodecylbenzene sulfonic acid (Sigma-Aldrich, USA) as a surfactant, and 1 vol.% (3-glycidyloxypropyl)trimethoxysilane (Sigma-Aldrich, USA) as a crosslinking agent to improve mechanical stability. PEDOT:PSS solution was spun on the selected areas of the substrate at 1 000 r.p.m. for 2 min and baked at 120 °C for 20 min. Before the operation the devices were conditioned at least 20 min in PBS solution, in order to avoid swelling effects during electrical measurements.

Fluid Chamber Fabrication: Fluid channels were prepared using a PMMA mold made by a micro-milling machine. PDMS was mixed with a crosslinker in a ratio of 10:1 wt/wt and degassed in a vacuum desiccator before being poured onto the mold and heated to 80 °C for 3 h to cure (PDMS, Sylgard 184). A 1.5 mm diameter biopsy punch was used to create the holes for inlets and outlets, which consisted of Teflon tubing (0.813 mm inner diameter, 1.32 mm outer diameter). A small amount of uncured PDMS was used to coat the bottom surface of the PDMS fluidic channel before placing it onto the glass-ITO substrate, which was subsequently baked at 80 °C for at least 1h.

Neurotransmitters' Solutions Preparation: Neurotransmitters' solutions were freshly prepared by dissolving dopamine hydrochloride (98%, Sigma-Aldrich, USA) and serotonin hydrochloride (98%, Sigma-Aldrich, USA) into Dulbecco's Phosphate Buffered Saline (Modified, without calcium chloride and magnesium chloride, Sigma-Aldrich, USA) at a different concentration ranging from 0.01 mM to 2 mM. Mixed neurotransmitters solutions were prepared by diluting single neurotransmitter ones.

Presynaptic – Gate Measurements: The electrochemical characterizations were performed by CV, DPV, and chronoamperometry techniques using an Autolab PGSTAT302N potentiostat/galvanostat (Metrohm AG, Switzerland) and the NOVA 1.8.14 software built-in routines. For these measurements, the ENODE channel was disconnected. The electrochemical potential values of the neurotransmitters reported in the manuscript

and in the Figure S3,S4,S5,S14,S15,S16 were measured with respect to a standard Ag/AgCl reference electrode while a Pt wire was used as the counter electrode (both terminals were inserted in the fluidic module). The ENODE gate PEDOT:PSS thin film was used as the working electrode. For CV measurements the potential was swept from -0.2 V to 0.6 V at variable scan rates ($1, 5, 10, 30, 50$ mV s $^{-1}$). For DPV, the instrumental variables were studied, and the optimum conditions resulted: pulse amplitude: 0.050 V; increment: 0.004 V; sample width: 4 s; pulse width: 5 s; pulse period: 10 s; sensitivity: 1×10^2 μ A. For chronoamperometry, the working electrode was subjected to different potential steps ($V = +0.3$ V for DA, $V = +0.4$ V for 5-HT, $V = +0.5$ V for AA) and the current response was measured for a period of 20 s with a sensitivity of 1×10^2 μ A.

Postsynaptic Measurements: Devices were characterized using 2 commercial platforms: ARKEO multichannel (located in TU/e Eindhoven) and ARKEO all-in-one (located in IIT Naples) developed by Cicci Research (Italy). These systems are composed of a thermal controlled stage, two fluidic pumps and two-channel and four-channel source meter units, respectively. The system (Eindhoven or Naples) used for various sets of experiments that are here presented is specified. Either needle or spring contact probes (as specified) were used to access the ENODE's gate and drain electrodes. The electrolyte flow across the device was controlled using two fluidic pumps (Syringe-pump) controlled by custom LabView software. To preliminary test the devices, transfer curves were taken by sweeping the presynaptic electrode voltage from -0.2 V to $+0.8$ V (V_G) while applying a constant $V_D = -0.1$ V on the postsynaptic electrode.

Optical measurements (ARKEO Multichannel): Excitation light was provided by a LED Tower (Cicci Research, Italy) (see Supplementary Figure S1) assembled on top of the Arkeo stage; the LED Tower comprises a set of 13 LEDs which allow to select, and combine, different excitation wavelengths. For all the performed experiments, a warm white light (range >4750 K) was used. Optical detection was performed with a CCD based spectrometer (360 – 1050 nm), multimode bundle, and a 10 mm diameter aspheric lens close to the substrate (access from the bottom of the Arkeo stage, see Figure S1, Supporting Information). The spot size was roughly 1 mm, and its position (indicated in Figure S1, Supporting Information) corresponds with the center of the channel area.

Amperometry In-Flow Measurements (ARKEO all-in-one): For these measurements, the ENODE channel was left unconnected. To the gate electrode, used as working electrode, potential steps were applied ($V = +0.3$ V for DA and $V = +0.4$ V for 5-HT) and the current response was measured for a period of 60 s. The fluidic module was preloaded with PBS solution. As the electrical measurement was started, the syringe pump was activated in sync by a Labview routine (flow rates tested were $0.1, 0.5, 0.7, 1, 1.3, 1.5, 1.7, 2$ mL min $^{-1}$) so that the selected PBS-NT solution was fluxed while monitoring the Ig with resolution of 0.02 ms.

Synaptic Weight Modulation & Reversibility In-Flow Experiments (ARKEO Multichannel): In this configuration, both the ENODE channel and gate electrodes were connected via needle probes. Pulsed measurements were performed using a set of voltage pulses on the gate (3 s ON, 10 s OFF) to target the oxidation of each NT ($V_G = +0.3$ V for DA, $V_G = +0.4$ V for 5-HT) while monitoring the postsynaptic conductance ($V_D = -0.1$ V). Simultaneously, the optical spectra were recorded via the coupled optical fiber.

For the static experiments (Figure 1), the fluidic module was preloaded with the solution PBS-neurotransmitter in exam, but the syringe pumps were not activated. After the set of pulses defining the learning protocol (50 s), the pumps were activated for fluxing PBS solution at 1 mL min $^{-1}$. Simultaneously, on the gate were applied three trains of voltage pulses with increasing amplitude (0.1 to 0.8 Vg, $\Delta V_G 0.1$ V, $V_D -0.1$ V) with a 120 s of delay while still monitoring the postsynaptic conductance ($V_D = -0.1$ V).

The device response was defined as the $\Delta G_D\%$ and $\Delta J/OD\%$ (see below section) measured 240 s after the end of the last train of pulses (800 s since the start of the measurement) while still fluxing PBS.

For pulsing-in-flow experiments (Figure 2, Figure S13, and Tables S4, Supporting Information), the fluidic module was preloaded with the solution PBS-NT in exam and a syringe containing the NTs solution was acti-

vated and set to the desired flow regime (from $0.5, 1, 1.5$ to 2 mL min $^{-1}$) 10 s before starting the opto-electronic measurement.

Synaptic Weight Modulation & Reversibility Parameters Extraction and Data Analysis: For the electronic readout in the used configuration, one channel the AKEO setup served to record the channel current. The measured current traces were converted into conductance by dividing them for the V_D applied on the channel (-0.1 V). To obtain the device electronic modulation from these traces, the point value of conductance at time 10 s (right before the start of the train of voltage pulses) was extracted as the "baseline conductance value" (reported in Figure S8,S9, Table S1, Supporting Information). Similarly, the point value of the conductance trace at time 45 s (5 s after the last pulse) was assumed as the after-modulation value. To better appreciate the electronic readout and reduce the device-to-device variations in baseline conductance, the conductance variations ΔG_D have been normalized by the "baseline conductance value" for each recorded trace (examined device). Thus, $\% \Delta G_D$ values are reported in the tables and in the main text for the electronic readout. Finally, the recovery of the electronic baseline has been extracted using the point value of the conductance at the time 800 s.

For the optical readout in the used configuration, the optical fiber records the transmitted light in counts through the device channel. Prior measurements, the fiber was calibrated by acquiring a spectrum in a no-light condition corresponding to the blank/dark (LED off) and a reference spectrum corresponding to the baseline value (LED on). In both conditions, the ENODE device was placed under the Tower LED on the Arkeo stage while the needle probes for electronic measurement were connected to the electrodes and the fluidic tubes were in place. As such, both the reference spectra consider that the LED probing light crosses the optical media corresponding to the fluidic module (PDMS septum) and the glass substrate.

The fiber counts acquisition trace from 360 to 1050 nm (full spectral data) was also converted, visualized on the ARKEO software (Cicci Research, Italy) and simultaneously saved as transmittance, absorbance, and integral of the absorbance in the region of interest (550 – 650 nm) for a live monitoring of the traces during the measurements.

Due to the activation of the fluidic pump after the modulation section of the experiment (50 s), in many experiments, the optical trace recorded over time (either transmittance, absorbance, or integral or absorbance) present some artifacts (jumps over scale of the recorded values) that are connected to the vibration of the PDMS section due to the incoming PBS solution flow. Following these spikes point-artifacts, the optical baseline might show a shift to slightly higher or lower values compared to the value recorded at 49 – 50 s (start of the PBS flow). Cleaning of the data was performed in order to restore the device baseline by applying a corrective shift to the optical traces after the spikes and jumps (100 s on) to match the baseline level values at 49 s. Thus, both the electronic and optical traces are visualized in the windows of conditioning (0 – 45 s) and recovery (100 – 800 s) where no artifacts are clearly present. Due to the intrinsic noise of the optical measurements, as reported in the SI, the optical traces ($\Delta J/OD$) have been smoothed by a smoothing box function with a factor of 5 in the range 0 – 45 s and a factor of 100 in the range 100 – 800 s. To obtain the "optical trace baseline value", the integral-of optical density $\Delta J/OD$ traces have been scaled to the arbitrary starting value of 0.1 in correspondence of the first point in the time scale before the start of the train of voltage pulses (time 9.7 s– 10.1 s, there is a short time-shift respect to the electronic reading). Then, the optical trace point values were averaged in the window 40 – 45 s (5 s after the last pulse) to obtain the after-modulation optical value. As in the case of the electronic readout (to reduce device-to-device variations), the variations $\Delta J/OD$ have been normalized by the initial J/OD . Thus, $\Delta J/OD\%$ values are reported in the tables and in the main text for the optical readout. Finally, the recovery of the optical baseline has been extracted using the average of the J/OD values in the window 750 – 800 s to reduce the device-to-device variations due to the intrinsic noise of these measurements.

All the values reported in the tables and in the graph of this manuscript are the result of an average over three replica experiments performed on three devices.

Transconductance Measurements (ARKEO all-in-one): In this configuration both the ENODE channel and gate electrode were connected to ARKEO all-in-one via spring probes. The gate potential was swept, replicating the CV protocol (from -0.2 to 0.6 V) while monitoring the G_D conductance. The transconductance was directly derived through a built-in Lab-view routine (Cicci Research, Italy). For static measurements, the fluidic module was preloaded with the examined solution while for in-flow experiments the syringe pump was activated 10s before starting the electrical measurement and kept active.

Supporting Information

Supporting Information is available from the Wiley Online Library or from the author.

Acknowledgements

The authors wish to thank Bas de Young (Cicci Research) for the support in developing the optical signal acquisition software. F.S. acknowledges the support of the European Research Council starting grant BRAIN-ACT No. 949478.

Open access funding enabled and organized by Projekt DEAL.

Conflict of Interest

The authors declare no conflict of interest.

Author Contributions

F.S. and Y.v.D.B. conceived the idea and supervised the project. G.M.M. carried out the device fabrication and the opto-electronical characterization. S.C. and G.M.M. proposed the methodology to perform the electrochemical analysis of neurotransmitters solution. G.M.M. and C.L. were responsible for the electrochemical characterization of the neurotransmitter interaction with the device. C.F. performed the simulation and modeling of neurotransmitter interaction with the gate electrode in different flow regimes. G.M.M., C.F., and U.B. were responsible for the interpretation of the transistor electrical characteristic. G.M.M., F.S., and Y.v.D.B. wrote the paper. All authors discussed the results and commented on the manuscript.

Data Availability Statement

The data that support the findings of this study are available from the corresponding author upon reasonable request.

Keywords

bio-hybrid synapses, optical absorption, organic mixed ionic-electronic conductors, organic electrochemical transistors

Received: December 20, 2022
Revised: March 6, 2023
Published online: April 23, 2023

- [1] K. Berggren, Q. Xia, K. K. Likharev, D. B. Strukov, H. Jiang, T. Mikolajick, D. Querlioz, M. Salinga, J. R. Erickson, S. Pi, F. Xiong, P. Lin, C. Li, Y. Chen, S. Xiong, B. D. Hoskins, M. W. Daniels, A. Madhavan, J. A. Liddle, J. J. McClelland, Y. Yang, J. Rupp, S. S. Nonnenmann, K.-T. Cheng, N. Gong, M. A. Lastras-Montañón, A. A. Talin, A. Salleo, B. J. Shastri, **2020**, 32, 46.

- [2] S. Furber, *J. Neural Eng.* **2016**, 13, 051001.
- [3] S. T. Keene, P. Gkoupidenis, Y. van de Burgt, in *Organic Flexible Electronics* (Eds.: P. Cosseddu, M. Caironi), Woodhead Publishing, **2021**, pp. 531–574.
- [4] T. V. P. Bliss, G. L. Collingridge, **1993**, 361, 9.
- [5] D. Marković, A. Mizrahi, D. Querlioz, J. Grollier, *Nat. Rev. Phys.* **2020**, 2, 499.
- [6] C. D. Schuman, S. R. Kulkarni, M. Parsa, J. P. Mitchell, P. Date, B. Kay, *Nat. Comput. Sci.* **2022**, 2, 10.
- [7] Y. van de Burgt, A. Melianas, S. T. Keene, G. Malliaras, A. Salleo, *Nat. Electron.* **2018**, 1, 386.
- [8] J. J. Yang, *Nat. Nanotechnol.* **2013**, 8, 13.
- [9] D. S. Jeong, K. M. Kim, S. Kim, B. J. Choi, C. S. Hwang, *Adv. Electron. Mater.* **2016**, 2, 1600090.
- [10] T. Someya, Z. Bao, G. G. Malliaras, *Nature* **2016**, 540, 379.
- [11] K.-N. Kim, M.-J. Sung, H.-L. Park, T.-W. Lee, *Adv. Electron. Mater.* **2022**, 8, 2100935.
- [12] A. Melianas, T. J. Quill, G. LeCroy, Y. Tuchman, H. v. Loo, S. T. Keene, A. Giovannitti, H. R. Lee, I. P. Maria, I. McCulloch, A. Salleo, *Sci. Adv.* **2020**, 6, eabb2958.
- [13] A. Gumyusenge, A. Melianas, S. T. Keene, A. Salleo, *Annu. Rev. Mater. Res.* **2021**, 51, 47.
- [14] J. Rivnay, S. Inal, A. Salleo, R. M. Owens, M. Berggren, G. G. Malliaras, *Nat. Rev. Mater.* **2018**, 3.
- [15] P. Gkoupidenis, N. Schaefer, B. Garlan, G. G. Malliaras, *Adv. Mater.* **2015**, 27, 7176.
- [16] M. Giordani, M. Berto, M. Di Lauro, C. A. Bortolotti, M. Zoli, F. Biscarini, *ACS Sens.* **2017**, 2, 1756.
- [17] S. T. Keene, *Nat. Mater.* **2020**, 19, 16.
- [18] X. Li, D. Bucher, F. Nadim, *J. Neurosci.* **2018**, 38, 8549.
- [19] E. Svensson, M. J. Williams, H. B. Schiöth, *Trends Neurosci.* **2018**, 41, 540.
- [20] P. Calabresi, B. Picconi, A. Tozzi, M. Di Filippo, *Trends Neurosci.* **2007**, 30, 211.
- [21] K.-P. Lesch, J. Waider, *Neuron* **2012**, 76, 175.
- [22] R. Kostrzewa, R. Brus, K. Perry, *Pol. J. Pharmacol.* **1999**, 51, 39.
- [23] F. S. Alfonso, Y. Zhou, E. Liu, A. F. McGuire, Y. Yang, H. Kantarci, D. Li, E. Copenhaver, J. B. Zuchero, H. Müller, B. Cui, *Proc. Natl. Acad. Sci. USA* **2020**, 117, 17260.
- [24] Y. Zhou, E. Liu, Y. Yang, F. S. Alfonso, B. Ahmed, K. Nakasone, C. Forró, H. Müller, B. Cui, *J. Am. Chem. Soc.* **2022**, 144, 23505.
- [25] N. F. Atta, A. Galal, R. A. Ahmed, *J. Electrochem. Soc.* **2011**, 158, F52.
- [26] I. Gualandi, D. Tonelli, F. Mariani, E. Scavetta, M. Marzocchi, B. Fraboni, *Sci. Rep.* **2016**, 6, 1.
- [27] T. Selvaraju, R. Ramaraj, *Electrochem. Commun.* **2003**, 5, 667.
- [28] J. Rivnay, S. Inal, B. A. Collins, M. Sessolo, E. Stavrinidou, X. Strakosas, C. Tassone, D. M. Delongchamp, G. G. Malliaras, *Nat. Commun.* **2016**, 7, 11287.
- [29] X. Ji, B. D. Paulsen, G. K. K. Chik, R. Wu, Y. Yin, P. K. L. Chan, J. Rivnay, *Nat. Commun.* **2021**, 12, 2480.
- [30] J. J. Langille, R. E. Brown, *Front Syst. Neurosci.* **2018**, 12, 52.
- [31] G. Kastellakis, D. J. Cai, S. C. Mednick, A. J. Silva, P. Poirazi, *Prog. Neurobiol.* **2015**, 126, 19.
- [32] A. Savva, S. Wustoni, S. Inal, *J. Mater. Chem. C* **2018**, 6, 12023.
- [33] A. E. Rodrigues, M. D. LeVan, D. Tondeur, Eds., *Adsorption: Science and Technology*, Springer Netherlands, Dordrecht **1989**.
- [34] N. Elgrishi, K. J. Rountree, B. D. McCarthy, E. S. Rountree, T. T. Eisenhart, J. L. Dempsey, *J. Chem. Educ.* **2018**, 95, 197.
- [35] F.-M. Zhou, Y. Liang, R. Salas, L. Zhang, M. De Biasi, J. A. Dani, *Neuron* **2005**, 46, 65.
- [36] D. Sun, H. Li, M. Li, C. Li, H. Dai, D. Sun, B. Yang, *Sens. Actuators, B* **2018**, 259, 433.